Geophysical Research Letters

RESEARCH LETTER
10.1029/2021GL095898

Key Points:

- Stratospheric aerosol levels were elevated to record levels over the entire Southern hemisphere for months following the Australian fires
- The fires caused warming uncorrelated between low latitudes versus extratropics, as in the volcanic eruptions of Pinatubo and El Chichon
- Ozone reduction was observed in midlatitude and polar regions, similar in magnitude to that following the Calbuco volcanic eruption in 2015

Correspondence to:
L. A. Rieger,
landon.rieger@usask.ca

Citation:
Rieger, L. A., Randel, W. J., Bourassa, A. E., & Solomon, S. (2021). Stratospheric temperature and ozone anomalies associated with the 2020 Australian New Year fires. *Geophysical Research Letters*, *48*, e2021GL095898. https://doi.org/10.1029/2021GL095898

Received 30 AUG 2021
Accepted 20 NOV 2021

Stratospheric Temperature and Ozone Anomalies Associated With the 2020 Australian New Year Fires

L. A. Rieger[1], W. J. Randel[2], A. E. Bourassa[1], and S. Solomon[3]

[1]Institute of Space and Atmospheric Studies, University of Saskatchewan, Saskatoon, SK, Canada, [2]National Center for Atmospheric Research, Boulder, CO, USA, [3]Department of Earth, Atmospheric, and Planetary Sciences, Massachusetts Institute of Technology, Cambridge, MA, USA

Abstract Stratospheric aerosol, temperature, and ozone anomalies after the 2020 Australian bushfires are documented from satellite observations. Aerosol extinction is enhanced in the Southern Hemisphere (SH) lower stratosphere (LS) in early 2020, comparable in magnitude to the Calbuco eruption in 2015. Warm temperature anomalies of 1–2 K occur in the SH LS during January-April 2020 and are coincident with enhanced aerosols. Radiative heating is indicated through anomalous temperature correlations between lower and higher latitudes. LS ozone shows midlatitude decreases several months after the aerosol maximum and before the polar vortex breakup, reaching extreme minima over the available OMPS record since 2011. Antarctic ozone depletion in the LS in 2020 reached a decadal low for both magnitude and persistence during November-December, along with record low polar temperatures and a strong polar vortex. Overall, the polar ozone depletion, temperature, and polar vortex evolution broadly resembled the effects of the Calbuco eruption in 2015.

Plain Language Summary The 2020 Australian forest fires injected a record amount of smoke into the stratosphere, similar in mass to recent, moderately sized volcanic eruptions. However, black carbon present in biomass burning plumes strongly absorbs incoming solar radiation leading to heating not seen after modest volcanic eruptions. This is evidenced by anomalous changes in temperatures at lower versus higher latitudes in the lower stratosphere compared to the last 40 years, eclipsed only by two of the largest volcanic eruptions. Aside from the temperature anomalies, stratospheric aerosol, ozone, and dynamics after the Australian fires show remarkable similarity to those following the Calbuco eruption. In the months following, ozone measurements show substantial low midlatitude anomalies indicating increased chemical destruction of ozone. Data from multiple satellites and model reanalyses reveal the global scale perturbations caused by forest fires, and the importance of understanding their chemical and dynamical influences.

1. Introduction

Unprecedented large bushfires in Eastern Australia during 29 December 2019 to 4 January 2020 (often referred to in the literature as the Australian New Year fires, or ANY) lofted smoke clouds into the lower stratosphere. Initial observations showed several distinct plumes in the lower stratosphere (LS), which could be traced over time and persisted in the stratosphere for several months (Kablick III et al., 2020; Khaykin et al., 2020; Peterson et al., 2020). These plumes displayed distinct chemical composition characteristic of biomass burning products (Boone et al., 2020; Schwartz et al., 2020), and solar heating of the most intense smoke plume resulted in induced heating, a self-generated anticyclonic circulation, and lofting of the plume to ~35 km (Allen et al., 2020; Kablick III et al., 2020; Khaykin et al., 2020; Schwartz et al., 2020). Estimates of the smoke injection from the ANY are 0.4–0.9 Tg (Khaykin et al., 2020; Peterson et al., 2020; Yu et al., 2021), likely considerably larger than stratospheric input from the British Columbia fires in 2017 which was estimated at 0.1–0.3 Tg (Peterson et al., 2018; Yu et al., 2019). In addition to the intense plumes, observations show zonal dispersion of the smoke clouds throughout the Southern Hemisphere (SH) LS, producing anomalously high aerosol optical depth for several months in early 2020 (Hirsch & Koren, 2021). Recently, Yu et al. (2021) presented model simulations of the bushfire smoke effects in the stratosphere, showing substantial warming of the LS coincident with the smoke, along with predicted LS ozone decreases from heterogeneous chemical reactions on the smoke aerosols. Yu et al. (2021) showed evidence of observed LS warming in early 2020 from MERRA-2 reanalyses (Gelaro et al., 2017), similar to the model prediction, but did not analyze ozone observations.

The objective of this paper is to present further observations of stratospheric aerosol, temperature and ozone responses to the ANY event using satellite data. This work places the effects of ANY in the context of comparable volcanic events of the previous decades and provides additional observational evidence for the radiative and chemical impacts investigated by the Yu et al. (2021) model study. We analyze aerosol extinction from the Ozone Mapping and Profiler Suite Limb Profiler (OMPS-LP) (Zawada et al., 2018) in order to quantify the ANY effects in the LS and compare with recent global variability. Further, LS temperatures from microwave measurements (so-called TLS temperatures), which are often used for climate monitoring (e.g., Steiner et al., 2020), clearly show the warming effects of the ANY aerosols. We also evaluate LS ozone variability from OMPS-LP and MLS (Livesey et al., 2020) to quantify how unusual the behavior in 2020 was, supporting the view that ozone changes associated with the unusual aerosol behavior is likely. Finally, observed aerosol, temperature and ozone variability in 2020 are compared with SH changes following the Calbuco volcanic eruption (near 41°S) in 2015, which had demonstrable effects on stratospheric ozone (Stone et al., 2017).

2. Data Analysis

2.1. TLS Temperature

We analyze temperature of the lower stratosphere (TLS) in this work using the v3.3 temperature anomaly data set from Remote Sensing Systems (RSS) (Mears & Wentz, 2009). This data set is derived from merged microwave satellite temperature measurements from MSU and AMSU, spanning from 1978 to present from a series of operational weather satellites. Details of the data are discussed at http://www.remss.com/measurements/upper-air-temperature/. The TLS product is sensitive primarily to temperatures from 13 to 22 km altitude, with approximately 20% of information coming from outside of this range (Mears & Wentz, 2009). For analysis, the RSS anomalies are detrended using a piecewise linear fit with a hinge-point at 1998.

2.2. MLS Temperature and Ozone

Launched in 2004 on the EOS AURA satellite, the Microwave Limb Sounder (MLS) continues to measure atmospheric emission in several microwave bands from the limb viewing geometry. The emission profiles are used to retrieve vertical profiles of many atmospheric species and parameters, including ozone and temperature. We use the version 5 temperature and ozone products (Livesey et al., 2020; Schwartz et al., 2008), which provide profiles from 261 hPa to above 1 hPa, with a vertical resolution of approximately 3–4 km.

2.3. OMPS-LP Aerosol and Ozone

The OMPS-LP instrument on the Suomi National Polar Orbiting satellite, which was launched in 2011, measures vertical images of the spectral radiance of the atmospheric limb. These scattered-sunlight spectra, in the range 290–1,000 nm, are used in combination with a radiative transfer forward model to retrieve vertical profiles of ozone number density and aerosol extinction coefficient. Measurements are made along the daylight portion of the satellite orbital track providing nearly global, daily coverage except for latitudes above 65° in midwinter. The OMPS-LP ozone and aerosol data products used in this work are derived using a two-dimensional, or tomographic, inversion enabled by the rapid image sampling of the instrument (Zawada et al., 2018). Aerosol extinction is retrieved at a single wavelength channel of 746 nm. The vertical and horizontal resolutions of the retrieval are approximately 1.5 and 250 km, respectively, and profiles generally extend from the tropopause through the upper stratosphere. OMPS-LP measurements have been used in previous studies of the impact of fire-generated aerosol on the stratosphere (e.g., Bourassa et al., 2019; Torres et al., 2020). While limb scattering aerosol retrievals are somewhat sensitive to underlying assumptions in the retrieval forward model, agreement with other limb scattering datasets from OSIRIS (Rieger et al., 2019) and occultation measurements from SAGE III/ISS (Damadeo et al., 2013) show good agreement, even under smoke conditions (Bourassa et al., 2019). Similar analysis was repeated for the ANY event, with comparable agreement between the three instruments. However, due to sampling, SAGE does not measure the initial plume, while OSIRIS loses coverage in the Southern hemisphere shortly thereafter; so while they provide excellent validation, they are not used further in this study.

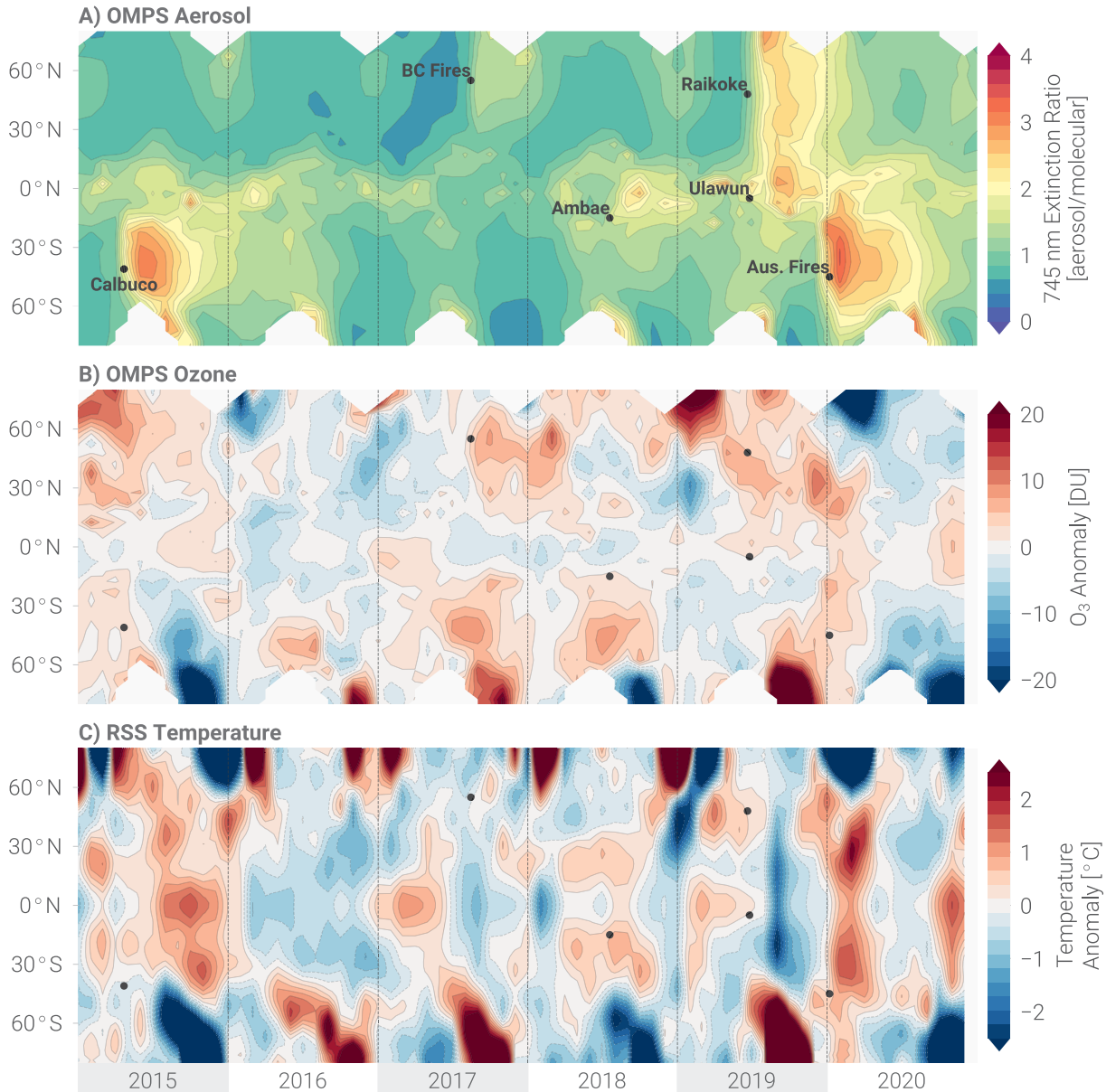

Figure 1. Latitude versus time sections of (a) Ozone Mapping and Profiler Suite Limb Profiler (OMPS-LP) lower stratosphere aerosol extinction, (b) OMPS-LP lower stratosphere ozone anomalies, and (c) temperature of the lower stratosphere (TLS) temperature anomalies. The aerosol extinction and ozone results are weighted for the lower stratosphere (approximately 13–22 km) using the TLS weighting function. Panel (a) indicates volcanic eruptions and large wildfire events impacting stratospheric aerosol. The ozone and temperature anomalies are calculated as deviations from the respective 2015–2020 seasonally varying averages.

3. Results

3.1. Aerosol and Temperature

Latitudinal structures of TLS anomalies during the recent few years (2015–2020) are shown together with LS aerosol extinction and LS ozone anomalies in Figure 1. Both the aerosol extinction and ozone anomalies are weighted in the vertical with the TLS weighting function, which peaks over ~13–22 km (Mears & Wentz, 2009). The OMPS-LP aerosol observations show a highly unusual maximum in 2020 tied to the ANY fires, along with episodic maxima linked to recent volcanic eruptions (Calbuco in 2015, Ambae in 2018, Ulawun and Raikoke in 2019), and a relatively smaller maximum from the British Columbia fires in 2017. These data show that the ANY fires produced a LS aerosol enhancement comparable to recent, moderate volcanic events, and that the aerosol ultimately covered most of the SH during 2020 (see Peterson et al., 2020).

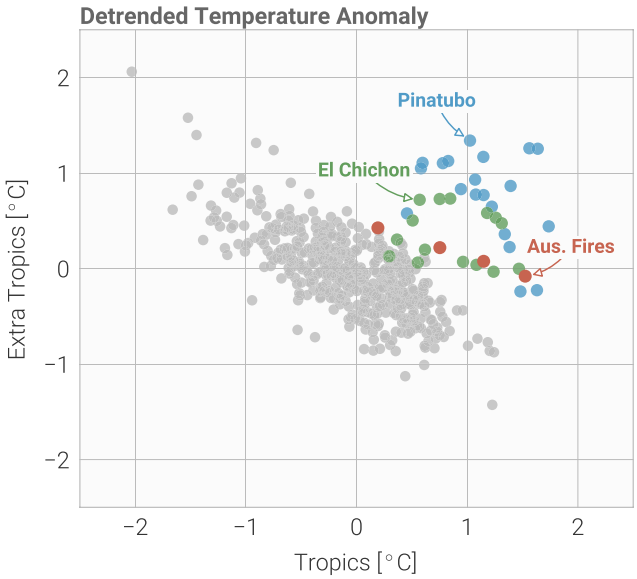

Figure 2. Scatter plot of monthly temperature of the lower stratosphere (TLS, approximately 13–22 km) temperature anomalies in the tropics (30°N-°S) and extratropics (>30° N/S) for each month during 1980–2020. Colored points correspond to the volcanic eruptions of Mt. Pinatubo (July 1991 to January 1993), El Chichon (May 1982 to February 1983), and the ANY fires (January 2020 to April 2020).

Global average TLS anomalies exhibit an anomalous short-term maximum ("spike") close to 1 K in early 2020 (Randel et al., 2021). Latitudinal structure of TLS anomalies (Figure 1c) show warm patterns in SH midlatitudes in early 2020, approximately overlapping the ANY aerosols (Figure 1a), but that signal is embedded within substantial year-to-year background variability, such as the early 2020 temperature increase in the NH. Much of the background variability is a reflection of large-scale circulation effects, often with equatorially centered structure linked with the quasi-biennial oscillation (QBO) (e.g., Baldwin et al., 2001). Mass balance implies that such dynamical fluctuations in the overturning circulation lead to anticorrelated temperature anomalies between lower and higher latitudes (e.g., Yulaeva et al., 1994). This behavior can be seen in Figure 1c, as polar temperature anomalies typically occur with low latitude maxima (e.g., SH events in 2019 and 2020, and in the NH during early 2020), as expected due to mass conservation. Figure 2 quantifies this behavior in the long TLS temperature record (1980–2020), showing systematic anticorrelation of extratropical (>30°N and °S) versus low latitude (30°N-S) temperature anomalies for the great majority of data. Anomalies deviate from this behavior prior to 2020 occur only during the major volcanic eruptions of El Chichon and Pinatubo, indicating the importance of radiative heating by the aerosols (e.g., Robock, 2000). The TLS anomalies during early 2020 also stand out in this diagnostic, with warm anomalies comparable to the El Chichon and Pinatubo volcanic eruptions, although the 2020 anomalies are much shorter lived. These latest warm anomalies that stand out in the context of purely dynamical variability are a fingerprint of diabatic heating from smoke aerosols (e.g., Yu et al., 2021).

Cross sections of the OMPS aerosol extinction and MLS temperature anomalies during January-April 2020 are shown in Figure 3. Enhanced ANY fire aerosols are observed in the SH LS beginning in January, with a maximum in February and slow decay of the LS maximum throughout 2020 (e.g., Figure 1a). During early 2020 the fire aerosols spread to SH polar regions and low latitudes, and by April the extratropical maximum appears to merge with the separate equatorial aerosol maximum that is a remnant of the 2019 Ulawun tropical volcanic eruption. The fire aerosols do not appear to propagate substantially beyond the tropics into the NH (Figure 1a). In addition to the hemispheric-scale LS aerosol enhancements, the OMPS measurements in February-April in Figure 3 show evidence of small-scale plumes that rise above the LS, extending above 30 km in March-April. These correspond to the concentrated self-rising smoke plumes discussed in Kablick III et al. (2020), Khaykin et al. (2020), Schwartz et al. (2020), and Allen et al. (2020). As a note, there is an additional aerosol maximum in the NH polar region in these months, which is likely a remnant of the Raikoke volcanic eruption in 2019, with possible contributions from 2019 Siberian fire smoke (Ohneiser et al., 2021).

Warm temperature anomalies of 1–2 K occur in the SH LS in Figure 3, approximately overlapping the enhanced SH aerosols, and these MLS results are similar to the results based on MERRA-2 reanalyses shown in Yu et al. (2021). Substantial warm anomalies (~3 K) also occur in the polar LS during February-March (somewhat below the TLS weighting function), causing record warm temperatures since 2011 in this region of normally low interannual variability. There are additional warm anomalies in the NH midlatitude LS seen in Figure 3, along with cold polar anomalies that are related to the record strong Arctic vortex in early 2020 (Lawrence et al., 2020). The coupled North-South temperature see-saw reflects the large-scale circulation patterns tied to the strong vortex, as discussed above (e.g., Yulaeva et al., 1994). While the NH midlatitude warm anomalies occur near the same time as the SH ANY effects (as seen also in Figure 2c), we view this as mostly a coincidence and not a direct effect of the aerosols.

3.2. Ozone

The idealized model calculations of Yu et al. (2021) assume that smoke aerosols become coated by sulfate and drive the same heterogeneous ozone chemistry as the latter. Their calculations suggest substantial ozone

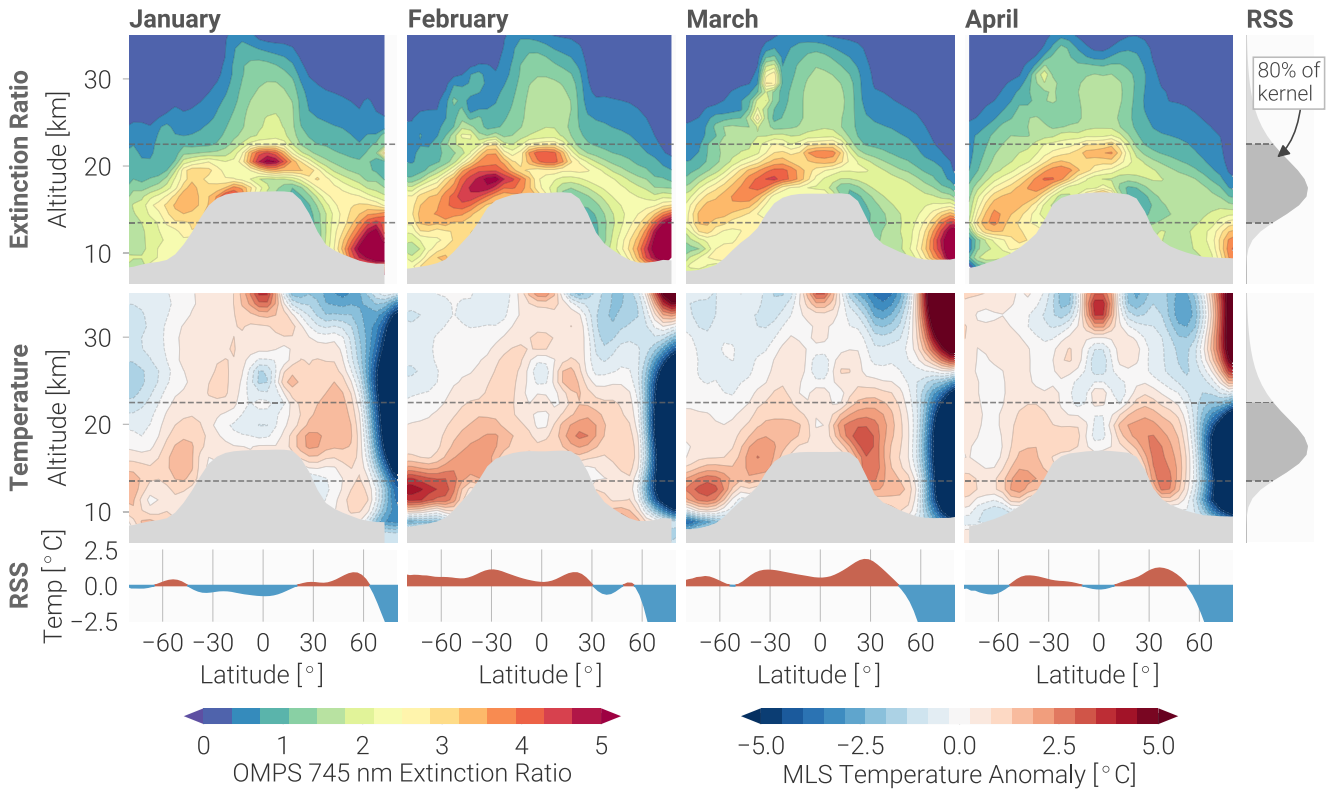

Figure 3. Cross sections of (top) Ozone Mapping and Profiler Suite Limb Profiler (OMPS-LP) aerosol extinction and (middle) Microwave Limb Sounder (MLS) temperature anomalies during January-April 2020. Temperature anomalies are calculated as deviations from the 2015 to 2020 average seasonal cycle, and the bottom panels show the corresponding temperature of the lower stratosphere (TLS) temperature anomalies. The TLS averaging kernel is indicated on the right, and the dashed black lines near 13 and 22 km indicate the central 80%.

depletion as a result of such aerosols, and hence it is interesting to examine the observational record in this regard. LS ozone anomalies in Figure 1b show substantial interannual variations that often mimic the LS temperature anomalies (Figure 1c), and this is well-known behavior that reflects large-scale circulation effects (e.g., Randel & Cobb, 1994). However, substantial negative LS ozone anomalies occur in 2020 in Figure 1b beginning in June over SH midlatitudes, and we note that these ozone anomalies are not reflected in coincident negative temperature anomalies, arguing against a dynamical cause. There are also strong negative ozone anomalies over polar regions during spring, when OMPS observations are available. Both the magnitude as well as latitudinal and seasonal patterns of the negative SH midlatitude ozone anomaly are similar to those obtained in the model calculations of Yu et al. (2021), again suggesting a chemical cause.

Variability of LS MLS temperatures, ozone, and OMPS-LP aerosol extinction is compared among recent years in Figure 4, contrasting the averages over midlatitude (30°–60°S) and polar (60°–90°S) regions. For this analysis, MLS ozone records are used to avoid loss of coverage in polar regions during winter; outside of polar winter the MLS and OMPS-LP ozone data show excellent agreement. Time series in Figure 4 highlight the distinctive behavior of 2020 contrasted to other years, together with the coupling among the different variables. We also highlight the year 2015 in Figure 4, when the Calbuco volcanic eruption occurred in April (near 41°S, see Figure 1a).

Midlatitude TLS anomalies in Figure 4a show warming during early 2020 that exceeds recent variability, and the signal vanishes after approximately April. Midlatitude 2020 LS ozone correspondingly displays the lowest values obtained in the distribution from May-July and is comparable to 2015 (the year of the Calbuco eruption) from October to December.

Polar latitudes show distinctive behavior during 2020, with similarities in aerosol, ozone, and temperature evolution to the observations during 2015. Enhanced aerosol extinction is observed in polar latitudes beginning in early 2020, and evidence of this rapid poleward transport from midlatitudes is also seen in Figure 3. Enhanced

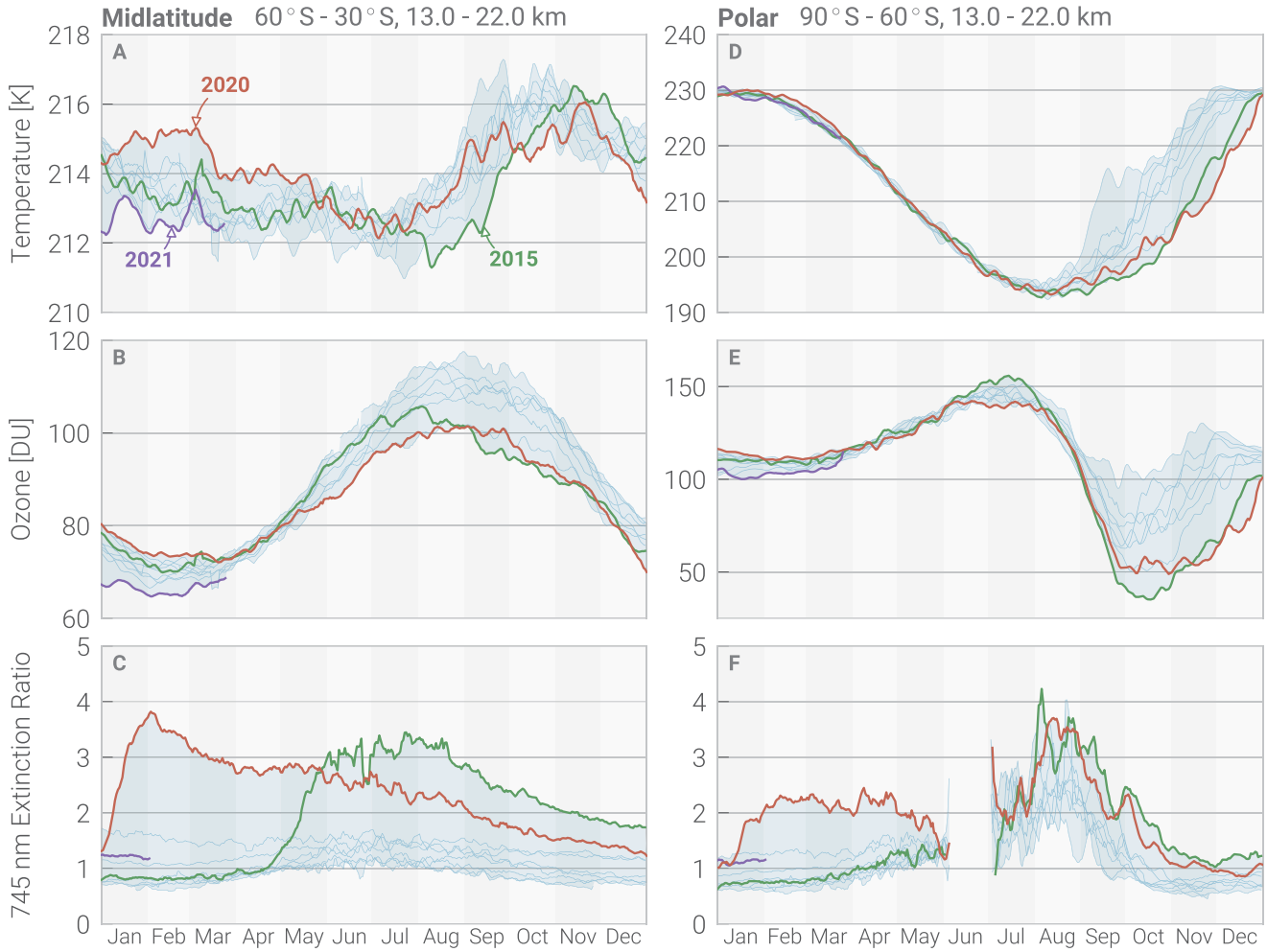

Figure 4. Time series of (top) temperature, (middle) Microwave Limb Sounder (MLS) lower stratosphere ozone, and (bottom) Ozone Mapping and Profiler Suite Limb Profiler (OMPS-LP) lower stratosphere aerosol extinction for each year over 2012–2020. Results are shown for averages over (left) 30°–60°S and (right) 60°–90°S. Color lines indicate the years 2015 (with the Calbuco eruption in April) and 2020–2021.

aerosols occur each year in Antarctic polar winter and spring associated with Polar Stratospheric Clouds (PSCs) (e.g., Pitts et al., 2018), and Figure 4f shows that polar aerosol extinction is anomalously high during October-December in both 2015 and 2020. However, note that in the polar region the OMPS-LP coverage is also seasonal, so that polar averages will be more heavily weighted to lower-latitude measurements as coverage is lost in the winter months (see Figure 1). LS polar ozone is anomalously low during both these years (Figure 4e), consistent with the unusually low values and extreme persistence of low ozone values through December in 2020 (https://public.wmo.int/en/media/news/record-breaking-2020-ozonehole-closes). These anomalously low ozone values are accompanied by record low polar stratospheric temperatures (Figure 4d) during November-December 2020. These low temperatures are likely strengthened, at least in part, by the reduction in radiative heating from the reduced ozone (Randel & Wu, 1999; Shine, 1986). In balance with the polar cooling, a stronger and more persistent polar vortex occurred in 2020 extending through the end of December (Figure 5), again similar to behavior in 2015. Overall, Figures 4 and 5 highlight remarkable similarity of the aerosol, ozone, temperature, and polar vortex evolution over the Antarctic during 2020 and 2015.

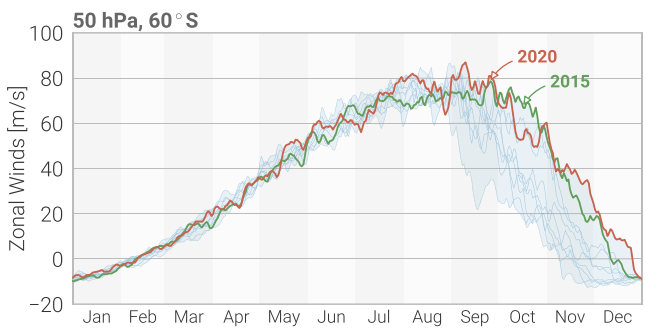

Figure 5. Daily time series of MERRA-2 zonal winds at 60°S and 50 hPa, showing the strength of the polar vortex. Blue lines indicate individual years between 2012 and 2021. Color lines indicate the years 2015 (with the Calbuco eruption in April) and 2020.

4. Summary and Discussion

In 2017, extreme forest fires in British Columbia created (at the time) record setting intrusions into the stratosphere (Bourassa et al., 2019). While considerably smaller than the ANY events, the aerosol reached altitudes of 22 km and persisted for months following the eruption. Although Yu et al. (2019) observed local reductions in ozone due to transport of tropospheric air, low ozone anomalies in 2017 are not apparent in the monthly and zonally averaged satellite observations (Figure 1b), contrasting with the comparatively large impact on ozone following the Australian fires. Additionally, the time delay of ozone loss after the ANY fires at this time (Figure 1c) suggests a chemical cause, as opposed to the transport of tropospheric air.

For comparable stratospheric impacts, we must look to the Southern hemisphere eruption of Mt. Calbuco in April of 2015. This eruption produced similar levels of aerosol, as well as midlatitude and polar LS ozone reduction during the following winter. This suggests that the chemical reactions occurring on the aged forest fire aerosols are similar, at least in midlatitude effects, to those of a volcanic eruption, despite the large difference in initial composition. This may point to comparable reaction rates, or to the biomass burning products becoming effectively coated in sulfuric acid and water, as suggested in Yu et al. (2021). Greater variability in polar dynamics and temperatures confounds confidence in a similar conclusion in the polar regions, although the comparison to Calbuco is suggestive. Further, Ohneiser et al. (2021) north polar wildfire smoke observations support a chemical ozone loss process. If intense wildfires increase in the twenty-first century as suggested by climate models (e.g., Abatzoglou & Williams, 2016), this study indicates that, at least in the next few decades, chemistry-climate-fire interactions may be an increasingly important factor when considering heterogeneous ozone loss.

Temperature anomalies of 1–2 K occurred in the SH LS in early 2020 in response to the ANY aerosols, and the signal stands out in global averages and low latitude versus higher latitude anticorrelation behavior similar to a large volcanic eruption, although shorter lived (Figure 2). The anomalous warming signal decayed after approximately 4 months. Corresponding zonal wind changes associated with the warming (via thermal wind balance) are relatively small, of order a few m/s, and probably do not strongly influence hemispheric-scale circulation throughout most of 2020. In Austral spring, an enhanced and persistent polar vortex, shown in Figure 5, and low temperatures may be linked to low polar ozone (Figure 4d) facilitated by the enhanced aerosol levels from the ANY fires.

Data Availability Statement

MLS temperature and ozone data were obtained from the Goddard Earth Sciences Data and Information Services Center at doi.org/10.5067/Aura/MLS/DATA2520 and doi.org/10.5067/Aura/MLS/DATA2516, respectively. MERRA-2 reanalysis products were obtained from the Goddard Earth Sciences Data and Information Services Center doi.org/10.5067/QBZ6MG944HW0. OMPS-LP ozone and aerosol products are available at doi.org/10.5281/zenodo.4014195, and doi.org/10.5281/zenodo.4029555, respectively. RSS temperature and related data were downloaded from http://www.remss.com/measurements/upper-air-temperature.

Acknowledgments
The National Center for Atmospheric Research is operated by the University Corporation for Atmospheric Research, under sponsorship of the US National Science Foundation. This work was partially supported by the NASA Aura Science Team under Grant 80NSSC20K0928. SS was supported by NSF Grants 1848863 and 1906719. LAR and AEB were supported in part by the Canadian Space Agency who provides ongoing funding to support the OSIRIS mission. We also thank the OMPS-LP team at NASA Goddard for producing and distributing high quality Level 1 radiances that are used to generate the L2 products used here.

References

Abatzoglou, J. T., & Williams, A. P. (2016). Impact of anthropogenic climate change on wildfire across western US forests. *Proceedings of the National Academy of Sciences of the United States of America*, *113*(42), 11770–11775. https://doi.org/10.1073/pnas.1607171113

Allen, D. R., Fromm, M. D., Kablick, G. P., III, & Nedoluha, G. E. (2020). Smoke with induced rotation and lofting (swirl) in the stratosphere. *Journal of the Atmospheric Sciences*, *77*(12), 4297–4316. https://doi.org/10.1175/jas-d-20-0131.1

Baldwin, M. P. (2001). The quasi-biennial oscillation. *Reviews of Geophysics*, *39*(2), 179–229. https://doi.org/10.1029/1999RG000073

Boone, C., Bernath, P. F., & Fromm, M. (2020). Pyrocumulonimbus stratospheric plume injections measured by the ace-fts. *Geophysical Research Letters*, *47*, 2020GL088442. https://doi.org/10.1029/2020GL088442

Bourassa, A. E., Rieger, L. A., Zawada, D. J., Khaykin, S., Thomason, L., & Degenstein, D. A. (2019). Satellite limb observations of unprecedented forest fire aerosol in the stratosphere. *Journal of Geophysical Research: Atmospheres*, *124*, 9510–9519. https://doi.org/10.1029/2019JD030607

Damadeo, R. P., Zawodny, J. M., Thomason, L. W., & Iyer, N. (2013). SAGE version 7.0 algorithm: Application to SAGE II. *Atmospheric Measurement Techniques*, *6*(12), 3539–3561. https://doi.org/10.5194/amt-6-3539-2013

Gelaro, R., McCarty, W., Suarez, M. J., Todling, R., Molod, A., & Takacs, L. (2017). The modern-era retrospective analysis for research and applications, version 2 (MERRA-2). *Journal of Climate*, *30*(14), 5419–5454. https://doi.org/10.1175/JCLI-D-16-0758.1

Hirsch, E., & Koren, I. (2021). Record-breaking aerosol levels explained by smoke injection into the stratosphere. *Science*, *371*(6535), 1269–1274. https://doi.org/10.1126/science.abe1415

Kablick, G., III, Allen, D. R., Fromm, M. D., & Nedoluha, G. E. (2020). Australian pyrocb smoke generates synoptic-scale stratospheric anticyclones. *Geophysical Research Letters*, *47*, e2020GL088101. https://doi.org/10.1029/2020GL088101

Khaykin, S., Legras, B., Bucci, S., Sellitto, P., Isaksen, L., & Tence, F. (2020). The 2019/20 australian wildfires generated a persistent smoke-charged vortex rising up to 35 km altitude. *Communications Earth & Environment*, *1*(1), 1–12. https://doi.org/10.1038/s43247-020-00022-5

Lawrence, Z. D., Perlwitz, J., Butler, A. H., Manney, G. L., Newman, P. A., Lee, S. H., & Nash, E. R. (2020). The remarkably strong arctic stratospheric polar vortex of winter 2020: Links to record-breaking Arctic oscillation and ozone loss. *Journal of Geophysical Research: Atmospheres*, *125*, e2020JD033271. https://doi.org/10.1029/2020JD033271

Livesey, N. J., Read, W. G., Wagner, P. A., Froidevaux, L., Santee, M. L., Schwartz, M. J., & Lay, R. R. (2020). *Version 5.0x level 2 and 3 data quality and description document*. (Tech. Rep. No. JPL D-105336 Rev. A).

Mears, C. A., & Wentz, F. J. (2009). Construction of the remote sensing systems v3.2 atmospheric temperature records from the MSU and AMSU microwave sounders. *Journal of Atmospheric and Oceanic Technology*, *26*(6), 1040–1056. https://doi.org/10.1175/2008jtecha1176.1

Ohneiser, K., Ansmann, A., Chudnovsky, A., Engelmann, R., Ritter, C., Veselovskii, I., et al. (2021). The unexpected smoke layer in the High Arctic winter stratosphere during MOSAiC 2019–2020. *Atmospheric Chemistry and Physics*, *21*(20), 15783–15808. https://doi.org/10.5194/acp-21-15783-2021

Peterson, D. A., Campbell, J. R., Hyer, E. J., Fromm, M. D., Kablick, G. P., Cossuth, J. H., & DeLand, M. T. (2018). Wildfire-driven thunderstorms cause a volcano-like stratospheric injection of smoke. *npj Climate and Atmospheric Science*, *1*(1), 1–8. https://doi.org/10.1038/s41612-018-0039-3

Peterson, D. A., Monterey, C., Campbell, J. R., Hyer, E. J., Fromm, M. D., Van, T., & Berman, M. (2020). *Quantifying the impact of intense pyroconvection on stratospheric aerosol loading*. Retrieved from https://ams.confex.com/ams/2020Annual/videogateway.cgi/id/521800?recordingid=521800

Pitts, M. C., Poole, L. R., & Gonzalez, R. (2018). Polar stratospheric cloud climatology based on CALIPSO spaceborne lidar measurements from 2006 to 2017. *Atmospheric Chemistry and Physics*, *18*(15), 10881–10913. https://doi.org/10.5194/acp-18-10881-2018

Randel, W. J., & Cobb, J. B. (1994). Coherent variations of monthly mean total ozone and lower stratospheric temperature. *Journal of Geophysical Research*, *99*(D3), 5433–5447. https://doi.org/10.1029/93JD03454

Randel, W. J., Covey, C., & Polvani, L. (2021). Stratospheric temperature and winds [in "State of the Climate in 2020"]. *Bulletin of the American Meteorological Society*, *102*(8), S27–S28. https://doi.org/10.1175/BAMS-D-21-0098.1

Randel, W. J., & Wu, F. (1999). Cooling of the Arctic and Antarctic polar stratospheres due to ozone depletion. *Journal of Climate*, *12*(5), 1467–1479. https://doi.org/10.1175/1520-0442(1999)012<1467:COTAAA>2.0.CO;2

Rieger, L., Zawada, D., Bourassa, A., & Degenstein, D. (2019). A multiwavelength retrieval approach for improved osiris aerosol extinction retrievals. *Journal of Geophysical Research: Atmospheres*, *124*, 7286–7307. https://doi.org/10.1029/2018JD029897

Robock, A. (2000). Volcanic eruptions and climate. *Reviews of Geophysics*, *38*(2), 191–219. https://doi.org/10.1029/1998RG000054

Schwartz, M., Lambert, A., Manney, G., Read, W., Livesey, N., & Froidevaux, L. (2008). Validation of the aura microwave limb sounder temperature and geopotential height measurements. *Journal of Geophysical Research*, *113*, D15S11. https://doi.org/10.1029/2007JD008783

Schwartz, M. J., Santee, M. L., Pumphrey, H. C., Manney, G. L., Lambert, A., Livesey, N. J., & Werner, F. (2020). Australian new year's pyrocb impact on stratospheric composition. *Geophysical Research Letters*, *47*, 2020GL090831. https://doi.org/10.1029/2020GL090831

Shine, K. P. (1986). On the modelled thermal response of the Antarctic stratosphere to a depletion of ozone. *Geophysical Research Letters*, *13*(12), 1331–1334. https://doi.org/10.1029/GL013i012p01331

Steiner, A., Ladstadter, F., Randel, W. J., Maycock, A. C., Fu, Q., & Claud, C. (2020). Observed temperature changes in the troposphere and stratosphere from 1979 to 2018. *Journal of Climate*, *33*(19), 8165–8194. https://doi.org/10.1175/JCLI-D-19-0998.1

Stone, K. A., Solomon, S., Kinnison, D. E., Pitts, M. C., Poole, L. R., & Mills, M. J. (2017). Observing the impact of calbuco volcanic aerosols on south polar ozone depletion in 2015. *Journal of Geophysical Research: Atmospheres*, *122*, 11862–11879. https://doi.org/10.1002/2017JD026987

Torres, O., Bhartia, P. K., Taha, G., Jethva, H., Das, S., Colarco, P., & Ahn, C. (2020). Stratospheric injection of massive smoke plume from Canadian boreal fires in 2017 as seen by DSCOVR-EPIC, CALIOP, and OMPS-LP observations. *Journal of Geophysical Research: Atmospheres*, *125*, e2020JD032579. https://doi.org/10.1029/2020JD032579

Yu, P., Davis, S. M., Toon, O. B., Portmann, R. W., Bardeen, C. G., Barnes, J. E., & Rosenlof, K. H. (2021). Persistent stratospheric warming due to 2019–2020 Australian wildfire smoke. *Geophysical Research Letters*, *48*, e2021GL092609. https://doi.org/10.1029/2021GL092609

Yu, P., Toon, O. B., Bardeen, C. G., Zhu, Y., Rosenlof, K. H., & Portmann, R. W. (2019). Black carbon lofts wildfire smoke high into the stratosphere to form a persistent plume. *Science*, *365*(6453), 587–590. https://doi.org/10.1126/science.aax1748

Yulaeva, E., Holton, J. R., & Wallace, J. M. (1994). On the cause of the annual cycle in tropical lower-stratospheric temperatures. *Journal of the Atmospheric Sciences*, *51*(2), 169–174. https://doi.org/10.1175/1520-0469(1994)051<0169:OTCOTA>2.0.CO;2

Zawada, D. J., Rieger, L. A., Bourassa, A. E., & Degenstein, D. A. (2018). Tomographic retrievals of ozone with the OMPS limb profiler: Algorithm description and preliminary results. *Atmospheric Measurement Techniques*, *11*(4), 2375–2393. https://doi.org/10.5194/amt-11-2375-2018